Ionospheric Electron Density Profiles Obtained With the Global Positioning System: Results From the GPS/MET Experiment

George Hajj and Larry Remans

Jet Propulsion Laboratory, California Institute of Technology

ABSTRACT

The GPS/MET experiment, which placed a GPS receiver in a low-Earth orbit tracking GPS satellites setting behind the Earth's limb, has collected data from several thousands of occultations since its launch in April 1995. This experiment demonstrated for the first time the use of GPS in obtaining profiles of electron density and other geophysical variables such as temperature, pressure and water vapor in the lower atmosphere. This paper presents a set of ionospheric profiles obtained from GPS/MET with the Abel inversion technique. The effects of the ionosphere on the GPS signal during occultation, such as bending and scintillation, are examined. Electron density profiles are obtained using the Abel inversion technique and compared to ones obtained from the Parametrized Ionospheric Model (PIM) and to ionosonde and incoherent scatter radar measurements. Statistical comparisons of N_mF_2 values obtained from GPS/MET and ionosondes indicate that these two types of measurements agree to -20% (1 sigma).

1. INTRODUCTION

In April, 1995, the GPS/MET (for GPS Meteorology) experiment placed a GPS receiver in a low-Earth orbit (LEO) tracking the global positioning system (GPS) satellites as they set behind the Earth's atmosphere. The basic concept of the GPS radio occultation technique is a simple one. When a signal transmitted by a GPS satellite and received by a LEO satellite passes through the Earth's atmosphere in a limb sounding geometry [Fig. 1], its phase and amplitude are affected in ways that are characteristic of the index of refraction of the medium along the path of propagation. By applying certain assumptions on the variability of the index of refraction of the propagating media (e.g. spherical symmetry in the locality of the occultation), phase change measurements between the transmitter and the receiver yield refractivity profiles in the ionosphere (-60-1000 km) and lower neutral atmosphere (0-60 km). The refractivity, in turn, yields electron density in the ionosphere, temperature and pressure in the neutral stratosphere and upper troposphere, and (with the aid of independent temperature data) water vapor density in the lower troposphere.

This method has been applied repeatedly in NASA's planetary occultation experiments [see e.g. Fjeldbo, 1971 and Tyler, 1987] and was inherited from the area of geological mapping of the Earth's interior. However, the application of the technique to sense the Earth's neutral atmosphere or ionosphere had to await the development of an infrastructure built for completely different purposes, namely, the set of 24 GPS satellites launched and maintained by the Department of Defense for the purpose of navigation. Once this set of satellites became operational, it became clear to some (e.g. Gurvich and Kasil'nikova [1987], Yunck et al. [1988]) that placing one receiver in LEO, with a full 360° field of view of the Earth's limb, will provide about 500 globally distributed occultations daily at a very low cost. This concept was tested for the first time with the GPS/MET experiment, managed by the University Corporation for Atmospheric Research (UCAR) [Ware et al., 1996], consisting of a 2 kg GPS receiver piggybacked on the

MicroLab I satellite having a circular orbit of 740 km altitude and 70° inclination. The GPS receiver is a space qualified TurboRogue [Meehan et al., 1992] capable of tracking up to 8 GPS satellites simultaneously at both frequencies transmitted by GPS. Due to the limited field of view of the GPS receiver's antenna and the onboard memory of the satellite, the GPS/MET collects anywhere between 100-200 globally distributed occultations daily. Since the start of the GPS/MET experiment in April of 1995, tens of thousands of occultations have been recorded by GPS/MET, providing a very rich data set to study the ionosphere and the lower neutral atmosphere.

Due to the abundance of neutral atmospheric data from radiosondes and the existence of accurate numerical weather models, several studies that examine the accuracies of temperature and pressure profiles obtain from GPS/MET have been published. For example, Kursinski et al. (1996) and Ware et al. (1996) demonstrated that GPS/MET temperature profiles are accurate to better than 1-2 K between -5-30 altitudes, while Leroy (1997) showed that geopotential heights of pressure levels in the same region are accurate to better than 20 meters. In the ionosphere, on the other hand, due to the sparsity of data, comparisons have been somewhat limited. In order to assess the accuracy of ionospheric electron densities derived from GPS occultations, several investigators have performed simulated experiments where synthetic data based on ionospheric models have been created and then inverted (see e.g. Hajj et al., 1994; Høeg et al., 1995; Decker et al., 1996; Leitinger et al. 1997). Those studies suggested several possible ways of inverting TEC data obtained from GPS occultations starting from the simplest approach of assuming a spherically symmetric medium and solving for an electron density profile for each occultation (e.g. Abel inversion approach presented below), to combining different occultations along with ground data to obtain 2-D or 3-D images of the ionosphere (tomographic inversions). While it is obvious that the assumption of spherical symmetry in the ionosphere is never an accurate one, the Abel inversion approach serves well as a starting point to understand some of the unique features associated with GPS occultation

data. The purpose of this paper is to examine some of these features and to estimate the accuracy of retrieved electron density profiles obtained with the Abel inversion by comparing to other independent measurements such as incoherent scatter radar and ionosondes. The accuracy obtained with this approach will be a lower bound on what can be achieved with more elaborate inversion methods.

The outline of the paper is as follows. Section two will briefly explain the Abel inversion technique as applicable to the ionosphere. Section three will examine some of the effects of the ionosphere on occulting signals, including bending and scintillation. Section four will present some results of electron density profiles, the coverage obtained with GPS/MET, and some comparisons to ionospheric models and to ionospheric measurements from incoherent scatter radars and ionosondes. Some conclusions are discussed in section five.

2. RADIO OCCULTATION TECHNIQUE—THE ABEL INVERSION

The basic observable for each occultation is the phase change between the transmitter and the receiver as the signal propagates through the ionosphere and the neutral atmosphere [Fig. 1]. A GPS phase measurement can be modeled as

$$\Phi = p + B^{trans} - B^{rec} + \Delta^{neutral} + \Delta^{iono} + b \qquad (1)$$

where p is the geometrical range, B^{trans} and B^{rec} are clock biases for the transmitter and the receiver, respectively, $\Delta^{neutral}$ and Δ^{iono} are the delays due to the neutral atmosphere and the ionosphere, and b is a phase ambiguity. In addition to the occulting GPS and LEO satellites, other measurements, taken from a network of ground receivers tracking GPS and from the LEO tracking other GPS satellites, are used to obtain precise orbit and clock

solutions of the satellites. The details of how the GPS/MET signal is calibrated in order to isolate the atmospheric effects on the occulting signals are given elsewhere [Hajj et al., 1995]. Here it suffices to say that through the calibration process the sum of the neutral and the ionospheric delays is isolated (up to a constant). For the occulting link going through the ionosphere, the neutral delay is negligible. This extra phase change induced by the medium is then differentiated (after proper smoothing) to obtain the extra Doppler shift induced by the medium. This extra Doppler shift can be used to derive the bending of the signal, et, as a function of the asymptote miss distance, *a*, [Fig. 1] by assuming a spherically symmetric atmosphere in the locality of the occultation; the relationship between the direction of the signal's propagation and the extra Doppler shift, Δf, *is* then given by

$$\Delta f = \frac{f}{c}\left[\vec{v}_t \cdot \hat{k}_t - \vec{v}_r \cdot \hat{k}_r - (\vec{v}_t - \vec{v}_r) \cdot \hat{k}\right], \tag{2}$$

where f is the operating frequency, c is the speed of light, $\vec{v}_t$ and $\vec{v}_r$ are the transmitter and receiver velocity respectively, $\hat{k}_t$ and $\hat{k}_r$ are the unit vectors in the direction of the transmitted and received signal respectively, and $\hat{k}$ is the unit vector in the direction of the straight line connecting the transmitter to the receiver. Assuming spherical symmetry introduces the extra constraint

$$a = n(\hat{r}_t)\left|\hat{r}_t \times \hat{k}_t\right| = n(\hat{r}_r)\left|\hat{r}_r \times \hat{k}_r\right| \tag{3}$$

where $\hat{r}_t$ and $\hat{r}_r$ are the coordinates of the transmitter and the receiver respectively, and n is the index of refraction at the specified coordinate. Eqs. (2) and (3) can be solved simultaneously in order to estimate the total atmospheric bending. Solving these two equations ideally requires knowledge of n at the satellites locations; however, in an

appendix we estimate that by setting $n = 1$ at the transmitter or the receiver (when *the* receiver is at reasonably high altitude, such as the case for the GPS/MET experiment), the solved-for ionospheric bending and the corresponding electron density are overestimated by no more than 0.5% of their true values. We proceed therefore by setting $n(\hat{r}_t) = n(\hat{r}_r) = 1$.

The spherical symmetry assumption can also be used to relate the signal's bending to the medium's index of refraction, n, via the relation [Born and Wolf, 1980, page 123]:

$$\alpha(a) = -2a \int_a^{\infty} \frac{1}{\sqrt{a'^2 - a^2}} \frac{\mathrm{din(n)}}{da'} da' , \qquad (4)$$

where $a = nr$ and r is the radius of the tangent point [Fig. 1]. This integral equation can then be inverted by using an Abel integral transform given by [see e.g. Tricomi, 1985, page 39]

$$\ln(n(a)) = -\frac{1}{\pi} \int_a^{\infty} \frac{\alpha(a')}{\sqrt{a'^2 - a^2}} da' . \qquad (5a)$$

The upper limit of the integral in Eq. (5) requires knowledge of the bending as a function of a all the way up to the top of the ionosphere. The GPS is above most of the ionosphere; however, this is not true of the GPS/MET instrument,at7110 km radius (740 km altitude). In order to obtain $\alpha(a)$ for $a > 7110$, an exponential extrapolation $\alpha(a)$ based on information from $a < 7110$ is used. In order to avoid dealing with the singularity at the lower bowndary of the integral, Eq. (5a) is rewritten as

$$\ln(n(a)) = -\frac{1}{\pi}\left[\alpha(a_{int})\ln\left(a_{int}+\sqrt{a_{int}^2-a^2}\right)-\alpha(a)\ln(a)-\int_a^{a_{int}}\ln\left(a'^2+\sqrt{a'^2-a^2}\right)\frac{d\alpha(a')}{da'}da'\right]$$

$$-\frac{1}{\pi}\int_{a_{int}}^{\infty}\frac{\alpha(a')}{\sqrt{a'^2-a^2}}da' \qquad (5.b)$$

where a_{int} is an intermediate value between a and co and is normally chosen to be slightly larger than a. The terms in bracket on the right hand side of Eq. (5.b) are the result of integration by parts.

In the ionosphere, the index of refraction is related to electron density via

$$n = 1 - 40.3\times\frac{n_e}{f^2} \qquad (6)$$

where n_e is the electron density in m^{-3} and f is the operating frequency in Hz. Eqs. (2)-(6) constitute the essence of the radio occultation profiling technique as it applies to the ionosphere. In the next two sections we will examine bending and electron density profiles derived with this technique.

3. IONOSPHERIC BENDING AND SCINTILLATION OF GPS OCCULTING SIGNALS

Data examined in this section were taken on May 4-5, 1995. During this period (and for much of the GPS/MET experiment) the L1 and L2 phase measurements for the occulting link were recorded once every 10 seconds when the tangent point was above -120 km altitude, and once every 20 msec (50 Hz rate) when the tangent point was below that height. This is because the GPS/MET experiment's primary goal is to sense the lower neutral atmosphere. Therefore, results presented in this and the next section will reflect a

rather coarse vertical resolution (-20-30 km) above ~120 km and a much finer vertical resolution (of order 1,5 km, corresponding to l/2-second smoothing in the processing) below -120 km altitude.

Based on Snell's law, the bending of the signal locally is in the direction of the refractivity gradient, In a general and approximate sense, the gradient of refractivity in the ionosphere is pointing upward above the F2 peak and downward below that peak. Therefore, the GPS signals will generally bend upward and downward above and below the F2 peak respectively. Examining the bending of the GPS L1 signal for 61 GPS/MET occultations that took place on May 4, 1995, we observe the following features [Fig. 2]:

1-The bending varies about two orders of magnitude between 0.0001-0.01 degrees (cannot be seen from the scale of Fig. 2) depending on local time and geographical location of the occultation. Since 1995 falls near a solar-minimum condition, the largest bending of figure 2 can be an order of magnitude smaller than the corresponding solar-maximum condition,

2-The highest peak in bending, which is associated with the F2 peak, varies in height between -250-400 km, consistent with F2 peak heights at different latitudes and local times.

3-With negative bending defined to be toward the earth, the signal bends away from (toward) the Earth above (below) well defined peaks in the ionosphere such as the F2 and the E peaks. Since the bending of the signal depends on the gradient of the refractivity (which is vertical, to first order), one expects to see a change of sign in the bending as the tangent point samples through a peak.

4-Very sharp variations of bending are associated with sporadic E layers. The largest absolute bending for this particular day is -0.03 degrees, which corresponds to the signal just descending below a sporadic E-layer. The fact that the bending induced by the sporadic E is larger than that of the F2 is due to the very short scale height associated with the sporadic E-layer, which makes the refractivity gradient largest there.

5-The tails at the bottom end of all these curves start to grow in magnitude due to the neutral atmospheric bending which dominates below about 50 km altitude.

The most striking feature of these data is how sharp the signature is around the E- (or sporadic E-) layer. Even though determination of the magnitude of the E-peak electron density might be obscured due to the overlaying layers and the assumption of spherical symmetry, the height of sharp E-layer appears to be reasonably well determined. However, no strong conclusion can be drawn on the accuracy of these heights without further analysis and simulation accounting for the E-layer variability being frequently quite regional and the effect of spherical symmetry assumption on the retrieval.

Bending for the L2 signal is a factor of 1.65 (= (154/120)2, the square of the ratio of L1 to L2 frequencies) larger than for L1 (see Eq. (6)). This dispersive nature of the ionosphere causes the L1 and L2 signals to travel slightly different paths and therefore sample different regions (as indicated by the solid and dashed lines in Fig. 1). This causes the tangent points of the two links to be at different heights in the atmosphere at a specific time. With the Abel inversion technique, the electron density profile and the height of the tangent point at a particular instant during the occultation can be solved for. Fig. 3 shows an example of an electron density retrieval obtained from GPS/MET for an occultation taking place near -6N latitude and 228E longitude around 20:04 UT of May 4, 1995 (the corresponding local time is 11:01). Also shown on the figure is the separation between the L1 and L2 tangent points as a function of altitude. In the neighborhood of the F2 peak, the relative position of the two signals change due to changing direction of bending. Above the F2 peak, since the bending is generally upward, the L2 tangent point will always be lower than the L1 tangent point The situation reverses when the signal tangent point is below the F2 peak. For this particular profile, the maximum separation is of order 300 meters; this scales linearly with the amount of bending a signal experiences. Therefore, one can expect separations that are two orders of magnitude smaller (as seen with the bending) or one order of magnitude larger during solar-max day-time. A large separation of the two signals

can be a limiting error for neutral atmospheric retrievals at altitudes above -40 km [Kursinski et al., 1997] unless higher order corrections are applied to calibrate for the ionosphere.

We now turn our attention to some amplitude data obtained from GPS/MET. Fig. 4 shows the flight receiver signal-to-noise ratio of the L1 and L2 signals for four different occultations, where time = O corresponds to the start of high-rate data at about 120 km altitude for each occultation. The gradual decrease of SNR starting at about 30-40 seconds is due to significant atmospheric bending starting at about the tropopause. As the signal approaches the surface, it bends significantly (up to - 10), defocuses and finally disappears. Nearly half of the occultation displays a smooth steady SNR while the signal is in the ionosphere. Figure 4.d is an example of such smooth SNR. However, a good fraction of them (see Fig. 4a, b and c) show one or several sharp changes in SNR which can be attributed to sharp layers (e.g. sporadic E) at the bottom of the ionosphere. That these scintillations are caused by the ionosphere and not the neutral atmosphere can be seen from the fact that the L2 SNR fluctuation is larger than that of L 1, consistent with its lower carrier frequency.

The electron density profiles obtained with the Abel inversion corresponding to the occultations of Fig. 4 are shown in Fig. 5. Fig. 5a, b and c respectively show one, several and two sharp layers at the bottom of the ionosphere.

4. OCCULTATION COVERAGE AND ELECTRON DENSITY PROFILING

As mentioned above, due to the antenna field-of-view ($\pm 30^{o}$) and memory limitations on board the satellite, only 100-200 occultations per day are collected from the GPS/MET. The coverage obtained during 20 days of the mission (April 24 and 25, May 3 and 4, June 21-24 and 27-30, July 1-7 of 1995) is shown in Fig. 6a, where each occultation is represented by one point (average location of geographic latitude and longitude of the

occultation tangent point). By contrast, the GPS/MET coverage for one day in sun-fixed coordinate is shown in Fig. 6.b where each line corresponds to one occultation intersecting the ionospheric shell between 100-400 km altitude.

Since the coverage In Fig. 6.b is shown as a function of sun-fixed longitude (O sun-fixed longitude corresponds to noon local time), and the occultations are scattered along the LEO orbit, the occultations are concentrated along the ground track of the GPS/MET satellite. At mid- and low-latitude the LEO samples the ionosphere at about the same latitude and local time for every revolution of the LEO orbit, This local time will precess slowly with the precession of the LEO orbit. For GPS/MET, it takes 110 days for a full precession of the satellite; therefore, it takes half of this period to sample the Earth at all local times for mid- and low-latitude. On the other hand, at high latitude, the same 12 hour period is sampled for a given hemisphere (e.g. in Fig. 6.b the northern hemisphere is always sampled between noon and midnight local time whereas the southern hemisphere is sampled between midnight and noon local time). It takes half of the precession period to reverse the sampling geometry.

The width of the spread of occultations around the LEO track is determined by the width of the field-of-view of the receiving antenna and the distance to the limb. For a 740 km altitude satellite (such as GPS/MET) the limb is about 3000 km away from the satellite. This implies that the tangent point of an occultation falls within a 3000 km radius from the satellite trajectory during that occultation, setting an upper limit on the width of the spread of occultations around the LEO track to be ~±27 equatorial degrees.

The reoccurrence of occultations at nearby local times and latitudes is illustrated by showing the retrievals of four equatorial occultations appearing at consecutive orbital revolutions, each taking place near noon local time. (These four occultations cross the circle in the middle of Fig. 6. b.) The electron density retrievals for these four occultations (using the Abel inversion) are shown in Fig. 7a.

For comparisons, profiles obtained from the Ionospheric Parametrized Model (PIM) [Daniell et al., 1995] derived with input parameters suitable for the same day are also shown. Some of the main features to observe are: (1) the ability to observe the E-, F1 - and F2-layers that are characteristic of mid- and low-latitude day-time ionosphere. (2) The ability to observe the evolution of the ionosphere at the same local time and latitude every -100 minutes (the GPS/MET orbital period) for mid- and low-latitude occultations. (3) Except for the far-left profile shown in 7a, the PIM reproduces F2 peak densities and heights that are in reasonable agreement with the GPS/MET retrieval. (4) Comparisons with the PIM is generally better below the F2-peak than at the top-side. (5) The ability of both the model and the retrievals to reproduce the sharp bottom of the ionosphere. Other examples of GPS/MET retrieved profiles are shown for high latitude between dusk and midnight local time in Fig. 7.b. We note the low F2-peak height, the near disappearance of the F1-peak, and the very low peak density near midnight local time (far-right in Fig. 7 b). In contrast to the equatorial profiles the comparison with the PIM model appears to be more favorable at the top-side than below the F2-peak.

Comparisons of GPS/MET profiles to ISR and ionosonde

In order to assess the accuracy of the GPS/MET retrievals, coincidences of other types of data such as ionosondes or incoherent scatter radar (ISR) with GPS/MET occultations have been examined, Fig. 8 .a shows a GPS/MET profile obtain on May 5, 1995, at about 0320 UT, with tangent points coordinates about 41 .9N and 282.3E (the tangent points for this occultation drifted between 40-43.8N and 281. 1-283.6E during the 4 minutes of the occultation). On the same figure are two ISR measurements of electron density obtained with a 640 microsecond pulse mode at about the same time and 20 minutes after the occultation. In Fig. 8.b the same GPS/MET profile is compared to an ISR profile obtained with a 320 microsecond pulse mode about 20 minutes after the occultation. Millstone Hill is located at 42.6N and 288.5E, which is about 6° east of the occultation location, The general agreement is fairly good, Discrepancies between the ISR and the

occultation can be ascribed to several factors, including the spatial separation between the occultation and the ISR measurements, error introduced by the spherical symmetry assumption when doing the GPS/MET retrieval, and the lower vertical resolution of the ISR measurements.

A more extensive comparison of N_mF_2 derived from f_oF_2 ionosonde measurements and GPS/MET profiles has been performed, with results shown in Fig. 9a. The comparison is between data obtained from a global network of ionosondes (Fig. 6a) and GPS occultations that took place within 1 hour and ~1100 km radius (corresponding to 10 degrees) from the ionosonde stations. The points shown on the figure correspond to all the coincidences found for the 20 day period of Fig. (6a). The middle line in Fig. 9.a corresponds to perfect agreement between these two measurements of N_mF_2. The upper and lower lines on the figure correspond to *+20%* and -20% deviation of GPS/MET derived N_mF_2 from the ionosonde N_mF_2 respectively. Differences in these two measurements are due to (1) error in the spherical symmetry assumption of the GPS/MET retrieval, (2) error in the ionosonde measurement, (3) spatial and temporal mismatch between the occultation time and location and those of the ionosonde. In order to better quantify these errors, we examine the fractional difference in N_mF_2, defined as

$$\delta = \frac{N_mF_2(\text{GPS/MET}) - N_mF_2(\text{ionosonde})}{N_mF_2(\text{ionosonde})} \qquad (7)$$

as a function of the separation distance between the two measurement, shown in Fig. 9 .b. There is an obvious growth in δ for larger separation distance. Limiting ourselves to measurements that are < 600 km apart (36 measurements out of 99), Fig. 10 shows a histogram of& which has a mean of 0.01, a standard deviation of 0.2 and a standard error in the mean of 0.03. The largest δ is 0.6.

5. DISCUSSION AND CONCLUSION

GPS occultations have been shown to provide a new and complementary vantage point over ground based measurements for probing the ionosphere. In the work described herein we have chosen to process bending obtained from a single frequency, which is possible through modeling the geometry and calibration of the receiver and transmitter clocks in the data-processing stage. Another approach, which is appropriate for ground-based or uncalibrated space-based measurements, would be to process the combination L1 -L2 (as done e.g. in Leitinger et al., 1997); this directly isolates the ionospheric delay, This dual-frequency approach has the advantages of being much simpler in principle because it eliminates the need for precise orbits and for transmitter and receiver clocks calibration, which in turn eliminates the need for simultaneous ground measurements. This simplicity however is at the cost of lower precision due to the noise added by L2, especially under conditions when the Department of Defense selective availability (SA) is turned on.

For the period analyzed (near solar minimum), bending in the ionosphere is on the order of 0.01 deg or less, with occasional stronger bending (up to 0.03 deg) occurring near sporadic E layers; this amount of bending implies a separation between the L1 and L2 signals of several hundred meters near the tangent point, At a period of solar maximum, these effects are expected to be an order of magnitude larger.

The strong vertical refractivity gradient at sporadic E layers causes strong scintillation and relatively large bending, which makes this technique potentially very useful for detecting the existence of these layers and their heights. However, further analysis that considers the effect of the spherical symmetry assumption on the retrieved profile is needed to determine the accuracy of these heights.

We have evaluated the accuracy of N_mF_2 measurements based on GPS/MET profiles by comparing with nearby ionosondes, when available. Based on the statistics

presented in section 4 above, we can conclude that N_mF_2 independently derived from GPS/MET retrievals and ionosonde measurements agree to within 20% (at the l-sigma level), and are essentially unbiased with respect to each other. This level of agreement is consistent with previous results [Hajj et al., 1994], where a simulation experiment indicated that N_mF_2 accuracy can be expected to be in the range of 0-50%, depending on the degree of non-sphericity encountered in the ionosphere.

With the assumption of spherical symmetry used in the Abel transform, the peak electron density is overestimated or underestimated at the tangent point, depending on whether the ionosphere at that point is at a relative minimum or a relative maximum, respectively. Linear (or higher odd) power gradients in the horizontal distribution do not influence the retrievals when spherical symmetry is assumed, simply because these terms cancel when integrated across an occultation link; only even terms in the gradient survive and appear as errors in the retrievals, Hajj et al. [1994] have shown that a significant improvement can be made to the spherical symmetry assumption by making use of global ground maps of vertically integrated TEC measurements such as those computed by Mannucci et al. [1997] The idea introduced there was to impose a horizontal gradient at each layer identical to that of the TEC map, and then solve for a scale factor for each layer. In this manner, each occultation is processed individually, but without assuming a spherically symmetric ionosphere. Alternatively, and more powerfully, one can combine nearby occultations along with ground links in order to perform 3-D tomography of the ionosphere [Hoeg et al., 1995; Hajj et al, 1996; Gorbunov et al., 1996; Leitinger et al., 1997].

Appendix

In this appendix we calculate the error in estimated bending due to setting the index of refraction to unity at the receiver's or transmitter's heights.

Consider the geometry of Fig. A below where the transmitting and receiving satellites are at radii R_t and R_r and travel with velocities V, and V_r respectively. The signal is transmitted in the direction of k, and received in the direction of k,. k is in the direction of the straight line connecting the transmitter and the receiver and corresponds to the direction that the signal would travel in vacuum. The extra Doppler shift caused by the intervening medium is then given by

$$\begin{aligned}\Delta f &= \frac{f}{c}\left(V_t\cos(\phi_t+\delta_t)+V_r\cos(\phi_r+\delta_r)\right)-\frac{f}{c}\left(V_t\cos\phi_t+V_r\cos\phi_r\right)\\ &= -\frac{f}{c}\left(V_t\sin(\phi_t)\delta_t+V_r\sin(\phi_r)\delta_r\right)\end{aligned} \tag{1}$$

where the angles are defined in Fig. A. In addition, the formula of Bouguer (Born and Wolf, 1980), valid for spherically symmetric media, implies

$$n_t\sin(\theta_t-\delta_t)R_t = n_r\sin(\theta_r-\delta_r)R_r \tag{2}$$

where n_t *and* n_r *are* the index of refraction at the transmitter and receiver respectively. Eqs. (1) and (2) are used to solve for δ_r and δ_t which correspond to the bending of the signal on each side of the occultation (see Fig. A). The total bending is the sum of these two terms,

In order to determine the error introduced by setting n_r and n_t to unity, we write Eq. (1) and (2) for n,= 1 + ε_t and n_r = 1 + ε_r (denoting the solution δ_r and δ_t) and then for n, = 1 and n_r = 1 (denoting the solution δ_t' and δ_r') and then subtract the two sets of equations. This procedure, after expanding Eqs. (1) and (2) to first order in δ_r ,δ_t and ignoring the small terms $\varepsilon_r\delta_r$ and $\varepsilon_t\delta_t$, leads to

$$V_t \sin(\phi_t)\Delta\delta_t + V_r \sin(\phi_r)\Delta\delta_r = 0 \qquad (3)$$

and

$$\cos(\theta_t)\Delta\delta_t R_t + \varepsilon_t \sin(\theta_t)R_t = \cos(\theta_r)\Delta\delta_r R_r + \varepsilon_r \sin(\theta_r)R_r \qquad (4)$$

where

$$\Delta\delta_t = \delta_t' - \delta_t \quad \text{and} \quad \Delta\delta_r = \delta_r' - \delta_r$$

Solving Eqs. (3) and (4), the error in the total bending Aa = $\Delta\delta_t + \Delta\delta_r$ is given by

$$\Delta\alpha = \frac{\left(\varepsilon_r \sin(\theta_r)R_r - \varepsilon_t \sin(\theta_t)R_t\right)\left(V_r \sin(\phi_r) - V_t \sin(\phi_t)\right)}{R_t \cos(\theta_t)V_r \sin(\phi_r) + R_r \cos(\theta_r)V_t \sin(\phi_t)} \qquad (5)$$

For GPS/MET geometry and a tangent height around 300 km, we have

$R_r = 7110$ km
$R_t = 26000$ km
$V_r = 7$ km/sec
$V_t = 3.8$ km/sec
$\theta_r = 70°$
$\theta_t = 15°$
$\phi_r = 20°$
$\phi_t = 75°$

Let $N_e(h_{LEO})$ be the electron density at the receiver's height, then $\varepsilon_r = (n - 1) = -40.3\, N_e(h_{LEO})/f^2$ (N_e is in m^{-3}, f is the radio frequency in Hz). At the GPS height we set $\varepsilon_t \approx$ O since the electron density is vanishingly small. Then, Eq. (5) reduces to

$$\Delta\alpha \equiv \alpha_{estimated} - \alpha_{true} = 0.123 \text{ X } \frac{40.3}{f^2} N_e(h_{LEO}) \qquad (6)$$

For $N_e(h_{LEO}) = 10^{,0}\, m^{-3}$ and $f = 1.57542$ Ghz, we get Aa = 1.1×10^{-6} deg.

Therefore, by ignoring the deviation of n from unity, we are overestimating the true bending caused by the ionosphere as derived from the GPS carrier phase measurements. (Note that we would be underestimating the bending by the same amount if we were to

derive it from the GPS pseudorange measurements since ε_r would have the opposite sign.)

Of importance is the bending error relative to the total bending. This fractional error can be approximated by using the following simple model for the ionosphere. Let

$$N_e(h) = N_{max} \exp\left(-\frac{h-h_{max}}{H}\right) \text{ for } h>h_{max} \text{ and O otherwise,}$$

where h_{max} and N_{max} correspond to the peak height and peak density respectively, H is the free electron density scale height, Then, to a good approximation, the total bending for a link with a tangent height $h > h_{max}$ *is* given by (Melbourne et al., 1994, page 47)

$$a(h) = \sqrt{\frac{2\pi R_{max}}{H}}\frac{40.3}{f^2}N_{max}\exp\left(-\frac{h-h_{max}}{H}\right) \quad (7)$$

where $R_{max} = h_{max}$ + radius of earth. The fractional bending error is then given by

$$\frac{\Delta\alpha}{\alpha}(h) = \frac{0\text{“ }1\ 2\ 3}{\sqrt{\frac{2\pi R_{max}}{H}}}\exp\left(-\frac{h_{LEO} - h}{H}\right) \quad (6)$$

For h_{LEO} = 740 km, R_{max} = *6670* km, *H = 70* km, we get

$$\frac{\Delta\alpha}{\alpha}(h) = 0.005\exp\left(-\frac{h_{LEO}-h}{H}\right).$$

Based on this exponential model and the GPS/MET geometry, bending is overestimated by less than 0.5% of the true one. In order to estimate the corresponding error in electron density, we use the differential form of the Abel transform integral (Eq. (5a) of section 2) which can be written as

$$\frac{\text{An}}{n} = -\frac{1}{\pi}\int_a^\infty \frac{\Delta\alpha}{\alpha}\frac{\alpha}{\sqrt{a'^2-a^2}}da' \quad (7)$$

using Eq. (6) in (7) it is easy to establish that

$$\frac{(N_e)_{estimated} - (N_e)_{true}}{(N_e)_{true}} < \frac{0.123}{2\pi R_{MAX}\sqrt{\frac{2\pi R_{MAX}}{H}}} \quad (8)$$

005

This implies that the derived electron density is overestimated by no more than 0.5% of the true density.

ACKNOWLEDGMENTS

We thank Mike Exner of UCAR for providing the GPS/MET flight data. We thank John Foster for providing the Millstone Hill ISR data. Ionosonde data were provided by the National Geophysical Data Center. This research was performed at the Jet Propulsion Laboratory, California Institute of Technology, under the JPL Director's Research Discretionary Fund with partial funding from the National Science Foundation.

REFERENCES

Born M. and Wolf E., *Principles of Optics*, Sixth edition, Pergamon Press, 1980.

Daniell R. E., L, D. Brown, D. N. Anderson, M. W. Fox, P. H. Doherty, D. T. Decher, J. J. Sojka, R. W. Schunk, "Parametrized Ionospheric Model-A global ionospheric parametrization based on first principles models," *Radio Science,* Vol. 30, No. 5, pp. 1499-1510, 1995.

Dekcer T. D., D. N. Anderson, R. M. Campbell, Simulations of GPS/MET Ionospheric Observations, Amer. Geophy. Union fall meeting, Dec. 1996.

Fjeldbo G. F., V. R. Eshleman, A. J. Kliore, "The neutral atmosphere of Venus as studied with the Mariner V radio occultation experiments," *Astron. J. 76,* pp. 123-140, 1971.

Gorbunov M. E., S. V. Sokolovsky, L. Bengtsson, *Space Refractive Tomography of the Atmosphere: Modeling of Direct and Inverse Problems,* Max-Planck-Institut fur Meteorologie, report No. 210, (ISSN 0937-1060), August, 1996.

Gurvich and Krasil'nikova, "Navigation Satellites for Radio Sensing of the Earth's Atmosphere", Sov. J. of Remote Sensing, 7, pp. 1124-1131, 1990.—Russian Original 1987.

Hajj G. A., R. Ibanez-Meier, E. R. Kursinski and L. J. Remans, "Imaging the Ionosphere with the Global Positioning System", *Int. J. of Imaging Sys. and Tech,,* Vol. 5, 174-184, 1994.

Hajj G. A., E. R. Kursinski, W. I. Bertiger, S. S. Leroy, and J. T. Schofield, "Sensing the Atmosphere From a Low-Earth Orbiter Tracking GPS: Early Results and Lessons From the GPS/MET Experiment," *Proc.* of ION-GPS 95, *The 8th International Technical Meeting of The Satellite Division of The Institute of Navigation,* pp 1167-1174, 1995.

Hajj G. A., L. Remans, W. Bertiger, R. Kursinski and T. Mannucci, "Imaging the ionosphere with GPS/MET", *proc. of the URSI GPS/MET Workshop,* Tucson, Arizona, Feb. 21-24, 1996.

H@eg P., A. Hauchecorne, G. Kirchengast, S. Syndergaard, B. Belloul, R, Leitinger, W. Rothleitner, Derivation of Atmospheric Properties Using . a Radio Occultation Techniques, *ESA/ESTEC Contract Rep. 11024/94 /NL/CN, DMI Sci. Rep. 95-4,* edited by P. Høeg and S. Syndergaard, Danish Meteorol. Int.t., Copenhagen, 1995.

Kursinski E. R., G. A. Hajj, K. R. Hardy, L. J. Remans, and J. T. Schofield, "Observing tropospheric water vapor by radio occultation using the global positioning system," *Geophy. Res. Lett.*, Vol. 22, No. 17, pp. 2365-2368, 1995.

Kursinski E. R, G. A. Hajj, W. I. Bertiger, S. S. Leroy, T. K. Meehan, L. J. Remans, J. T. Schofield, D. J. McCleese, W. G. Melbourne, C. L. Thornton, T. P. Yunck, J. R. Eyre and R. N. Nagatani, "Initial Results of Radio Occultation Observations of Earth's Atmosphere Using the Global Positioning System," *Science,* Vol. 271, pp. 1107-1110, 1996.

Kursinski E. R., G. A. Hajj, K. R. Hardy, J. T. Schofield, and R. Linfield, "Observing Earth's Atmosphere with Radio Occultation Measurements using GPS," *J. Geophys. Res.,* in press, 1997.

Leitinger R., H. P. Ladreiter and G. Kirchengast, "Ionosphere tomography with data from satellite reception of global navigation satellites signals and ground reception of navy navigation satellite system signals", *Radio Science, v32 (4),* pp1657- *1669, 1997.*

Leroy S., "The Measurement of Geopotential Heights by GPS Radio Occultation," submitted to *J. Geophys. Res.*, Vol. 102, No. D6, pp. 6971-6986, 1997.

Mannucci A. J., B. D. Wilson, D. N. Yuan, C. M. Ho, U. J. Lindqwister, T. F. Runge, "A Global Mapping Technique for GPS-Derived Ionospheric TEC Measurements," submitted to *Radio Science,* 1997.

Meehan T.K. et al., "The TurboRogue GPS Receiver", *6th Int. Geodetic Symp. on Satellite Positioning,* Columbus Ohio, 1992.

Melbourne W. G., E. S. Davis, C. B. Duncan, G. A. Hajj, K. R. Hardy, E. R. Kursinski, T. K, Meehan, L. E. Young, T. P. Yunck, *The Application of Spaceborne*

GPS to Atmospheric Limb Sounding and Global Change Monitoring, Jet Propulsion Laboratory publication 94-18, April 1994.

Tricomi F. G., *Integral Equations,* Dover Publications, Inc., New York, 1985.

Tyler G. L., "Radio propagation experiments in the outer solar system with Voyager," *Proc. IEEE, 75:1404-1431,* 1987.

Ware R., M. Exner, D. Feng, M. Gorbunov, K. Hardy, B. Herman, Y. Kuo, T. Meehan, W. Melbourne, C. Rocken, W. Schreiner, S. Sokolovskiy, F. Solheim, X. Zou, R. Anthes, S. Businger, and K. Trenberth. "GPS sounding of the atmosphere from low earth orbit: preliminary results," *Bulletin of the American Meteorological Society,* Vol. 77, No. 1, pp. 19-40, 1996.

Yunck T. P., G. F. Lindal and C. H. Liu, "The Role of GPS in precise earth observation," in Proceedings of the IEEE Position, Location and Navigation Symposium, Orlando, Florida, 1988.

FIGURE CAPTIONS

Figure 1: Occultation geometry defining a, r, α and the tangent point and showing the separation of the L 1 and L2 signals due to the dispersive ionosphere.

Figure 2: Bending induced by the ionosphere and neutral atmosphere on the L1 signal for 61 globally distributed occultations on May 4, 1995. Negative bending is defined to be toward the Earth's center.

Figure 3: Electron density retrieved from occultation and the corresponding amount of L1 and L2 signal vertical separation at the tangent point.

Figure 4: Instrumental signal-to-noise ratio as a function of time for L1 and L2 signals for four different occultations.

Figure 5: GPS/MET profiles of electron density corresponding to the occultations of Fig. 4 and indicating the ability of GPS occultations to resolve sharp layers in the ionosphere.

Figure 6. (a) GPS/MET coverage in geographic coordinates for 20 days (April 24 and 25, May 3 and 4, June 21-24 and 27-30, July 1-7 of 1995). Each dot indicates the location of the tangent point of the occultation when it is at -100 km altitude. The triangles indicate locations of ionosonde stations used in order to compare to N_mF_2 derived from GPS/MET. (b) GPS/MET coverage in sun-fixed coordinates in 24 hours, May 4, 1995. Each connected line corresponds to the ground projection of an occultation link when the tangent point (middle of the line) is at 100 km altitude. The ends of the line correspond to points on that same link at 400 km altitudes. At low latitude, the occultations sample roughly the same local time and same latitude every orbital revolution. The circle indicates four

occultations corresponding to four consecutive orbital revolutions (-100 minutes apart); the corresponding profiles are shown in Fig. 7a.

Figure 7: Examples of electron density profiles (e/m^3) obtained from GPS/MET and PIM for May 4, 1995. (a): low latitudes profiles (b): high latitudes profiles. Indicated on the top of each profile are universal time, local time, latitude and longitude of each occultation.

Figure 8: Comparisons of an electron density profile obtained from GPS/MET on May 5, 1995,0320 UT, with nearby measurements from Millstone Hill ISR. (a): GPS/MET vs. two ISR measurements with 640 μs pulse mode at 0321 UT and 0340 UT. (b) GPS/MET vs. ISR measurements with 320 μs pulse mode at 0341 UT. The occultation tangent point is about 6° west and 1° south of Millstone Hill.

Figure 9a: A scatter plot of N_mF_2 derived from ionosonde measurements of F_oF_2, and GPS/MET electron density profiles, showing the degree of correlation between the two. The middle line corresponds to perfect correlation; the upper and lower lines bound of the region of 20% deviation in the two measurements.

Figure 9.b: The fractional difference between N_mF_2 derived from GPS/MET and the ionosonde (defined in Eq. (7)) as a function of the distance between the station and the tangent point of the occultation. Differences that are larger than -0.5 can be attributed to the large distance between the station and the occultation.

Figure 10: Histogram of the fractional difference between N_mF_2 derived from GPS/MET and the ionosonde for measurements within 1 hour and 600 km from each other. Average and standard deviation are 0.01 and 0.20 respectively. Based on this histogram, the two

independent measurements of N_mF_2 agree to within 20% (1-sigma) and are essential unbiased.

Figure A: Geometry showing the direct line-of-sight between transmitter and receiver and the asymptotes of transmitted and received signals.

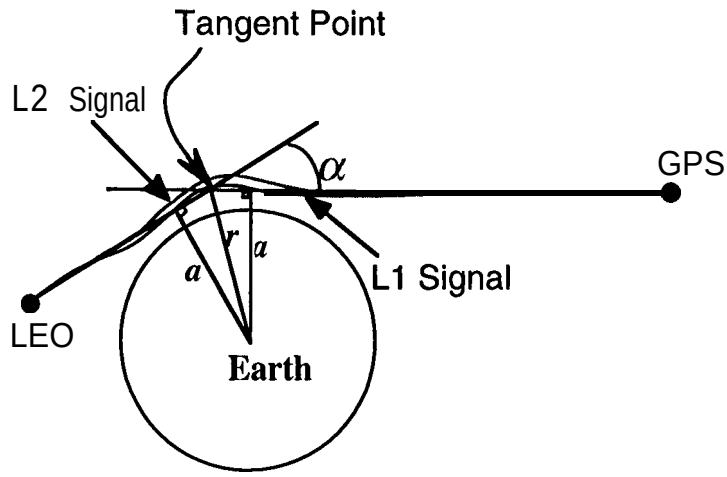

Figure 1

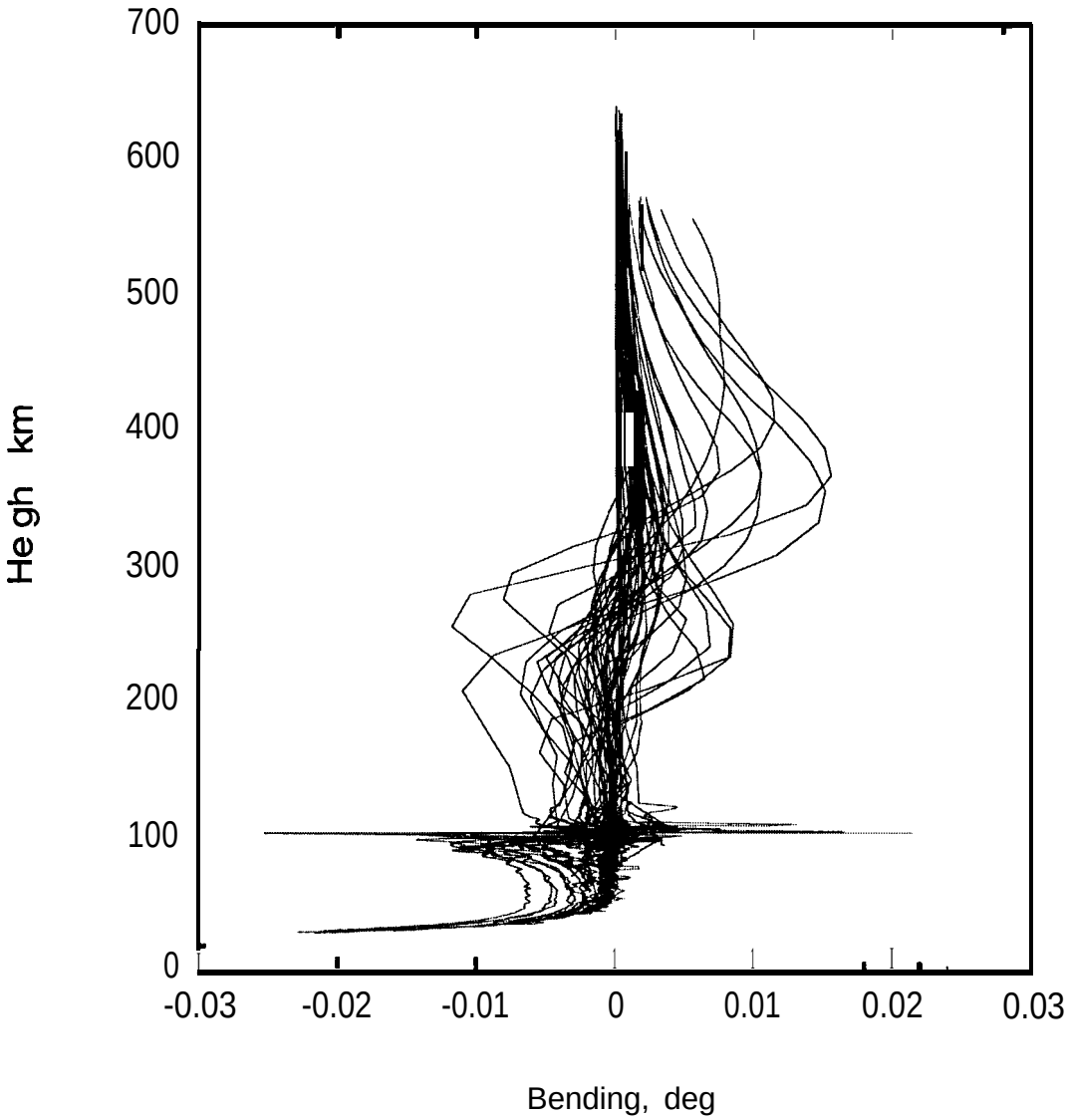
700
600
500
400
300
200
100
0
Height km
-0.03
-0.02
-0.01
0
0.01
0.02
0.03
Bending, deg

Figure 2

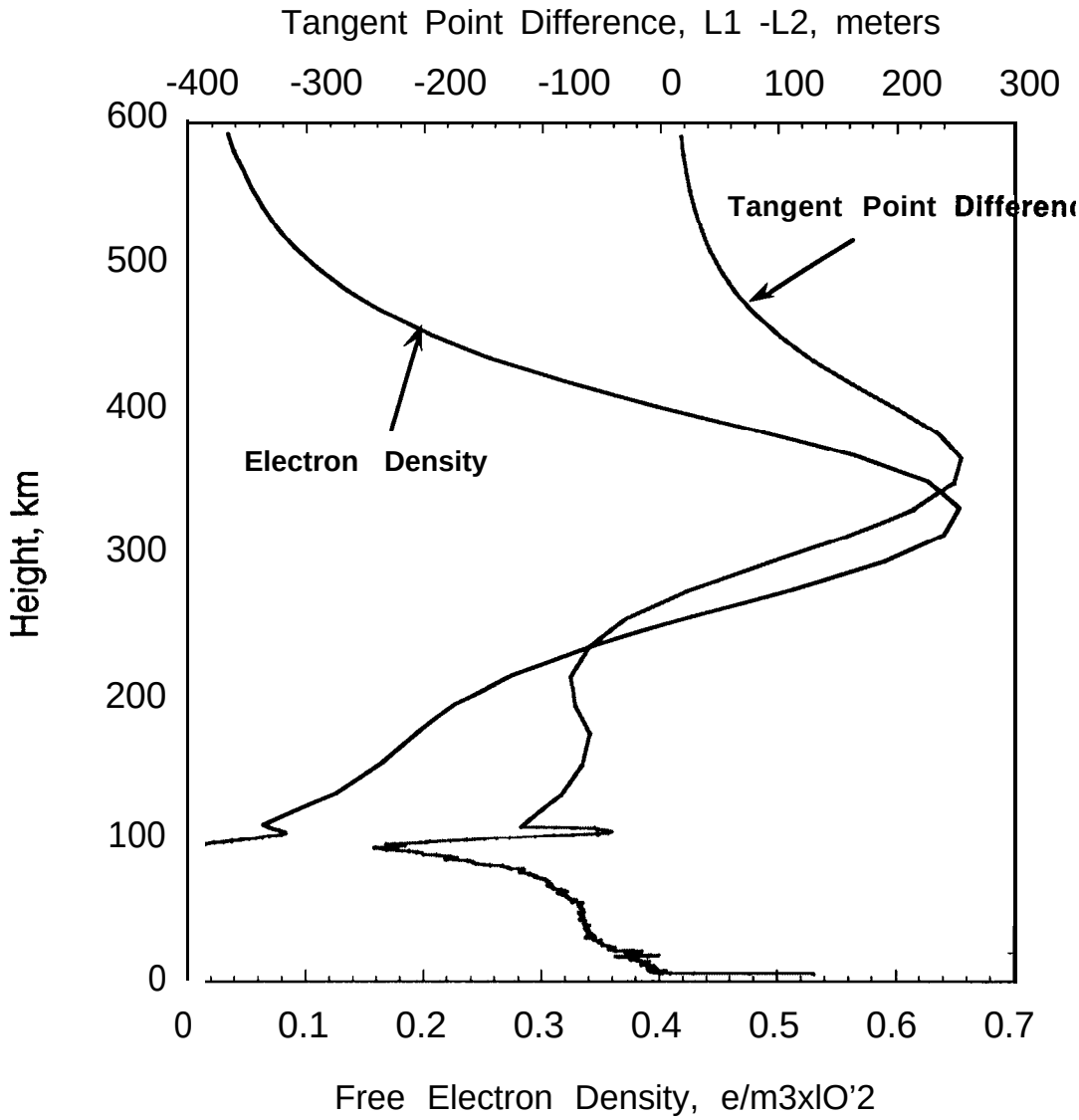
Tangent Point Difference, L1 -L2, meters
-400
-300
-200
-100
0
100
200
300
600
500
400
300
200
100
0
Height, km
Tangent Point Differenc
Electron Density
0
0.1
0.2
0.3
0.4
0.5
0.6
0.7
Free Electron Density, e/m3xlO'2

Figure 3

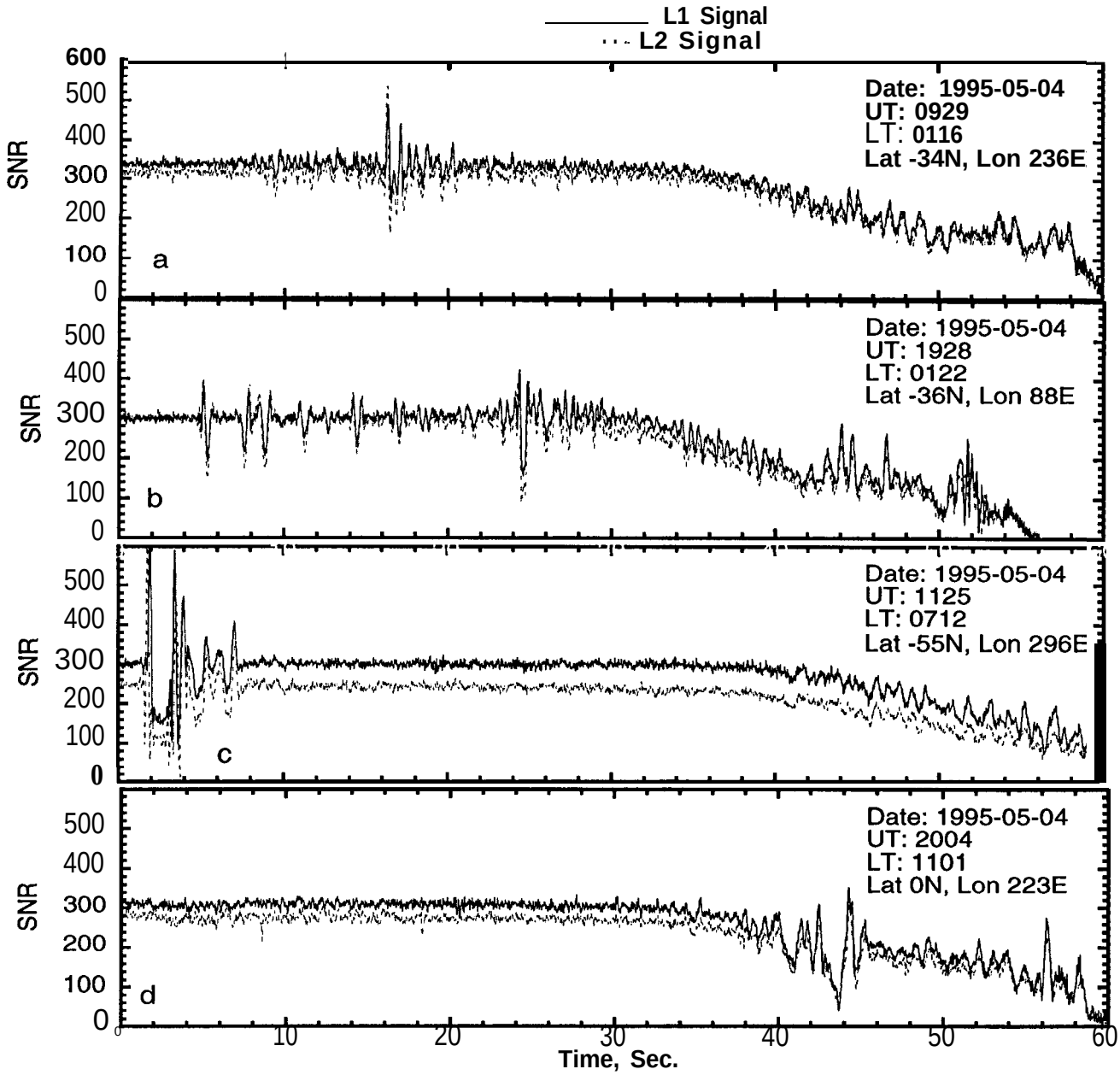
L1 Signal
L2 Signal
SNR
Date: 1995-05-04
UT: 0929
LT: 0116
Lat -34N, Lon 236E
a
Date: 1995-05-04
UT: 1928
LT: 0122
Lat -36N, Lon 88E
b
Date: 1995-05-04
UT: 1125
LT: 0712
Lat -55N, Lon 296E
c
Date: 1995-05-04
UT: 2004
LT: 1101
Lat 0N, Lon 223E
d
0
100
200
300
400
500
600
10
20
30
40
50
60
Time, Sec.

Figure 4

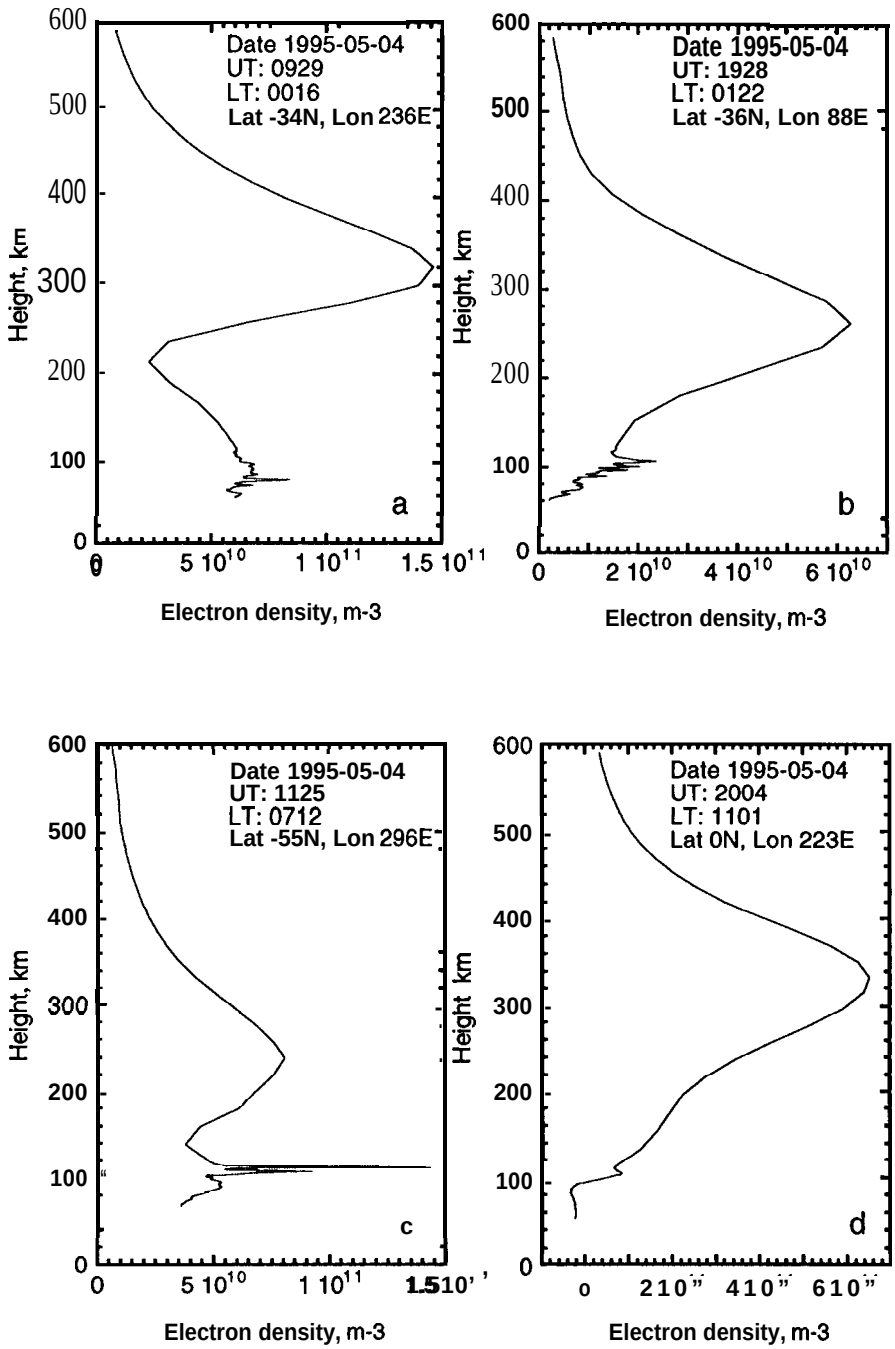
Date 1995-05-04
UT: 0929
LT: 0016
Lat -34N, Lon 236E
a
Date 1995-05-04
UT: 1928
LT: 0122
Lat -36N, Lon 88E
b
Date 1995-05-04
UT: 1125
LT: 0712
Lat -55N, Lon 296E
c
Date 1995-05-04
UT: 2004
LT: 1101
Lat 0N, Lon 223E
d
Height, km
Electron density, m-3
0
100
200
300
400
500
600
5 10^10
1 10^11
1.5 10^11
2 10^10
4 10^10
6 10^10

Figure 5

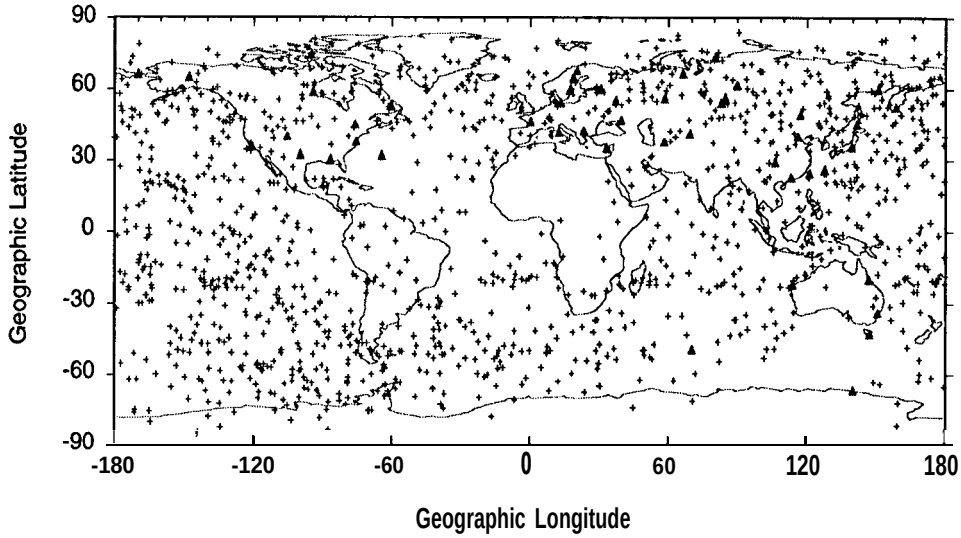
90
60
30
0
-30
-60
-90
Geographic Latitude
-180
-120
-60
0
60
120
180
Geographic Longitude

(a)

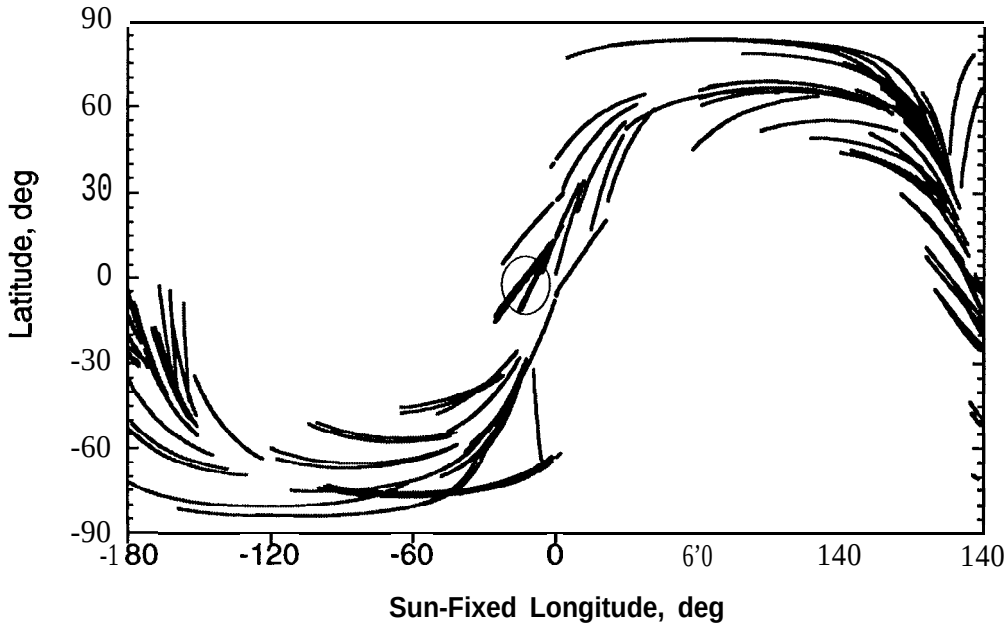
90
60
30
0
-30
-60
-90
Latitude, deg
-180
-120
-60
0
60
140
140
Sun-Fixed Longitude, deg

(b)

Figure 6

ELECTRON DENSITY PROFILES FROM GPS/MET AND THE PARAMETRIZED IONOSPHERIC MODEL OBTAINED FOR MAY 4, 1995 AT ABOUT THE SAME LATITUDE AND LOCAL TIME

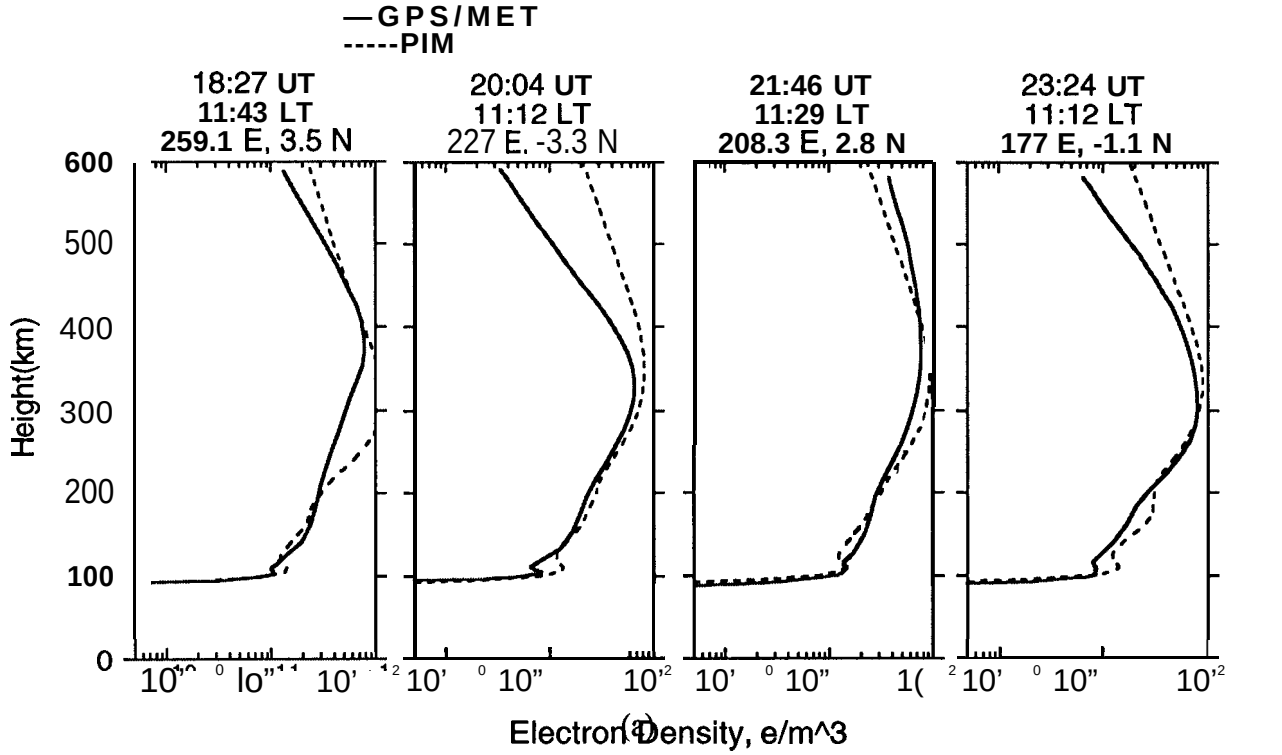

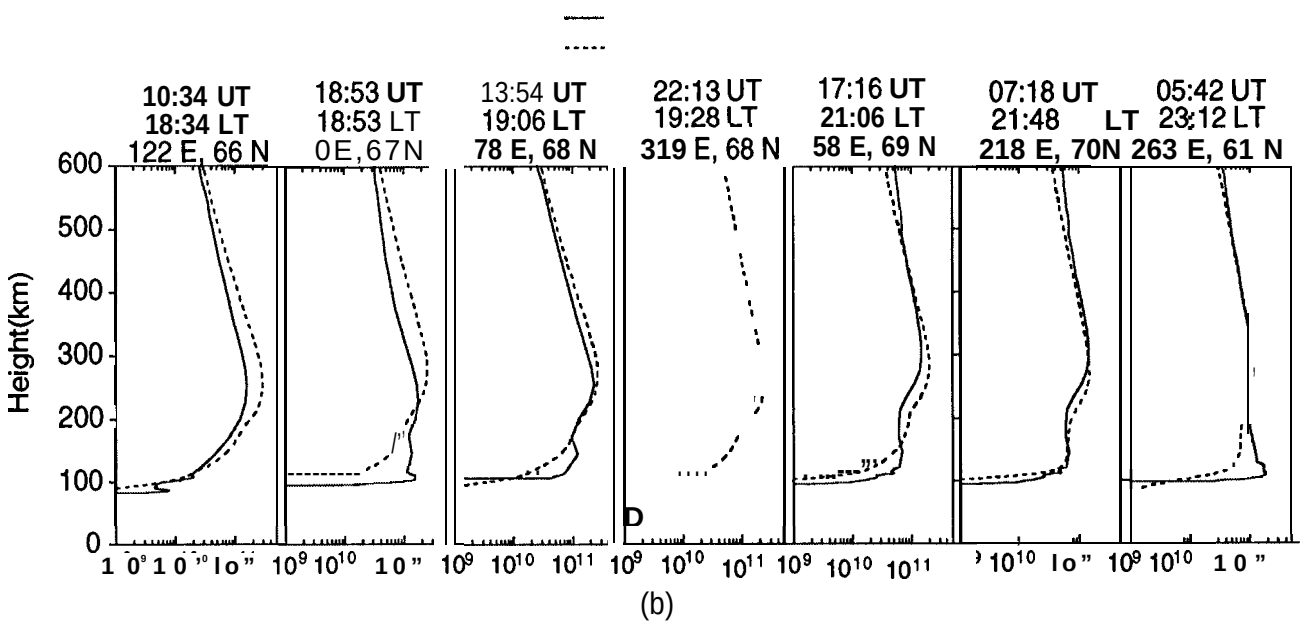

Figure 7

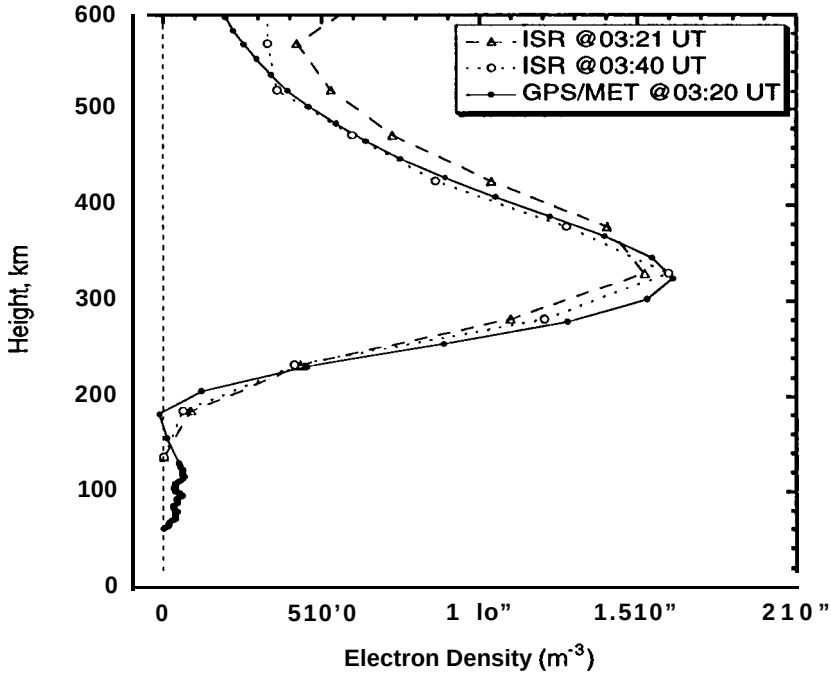
ISR @03:21 UT
ISR @03:40 UT
GPS/MET @03:20 UT
Height, km
600
500
400
300
200
100
0
0
510'0
1 lo"
1.510"
210"
Electron Density (m-3)

(a)

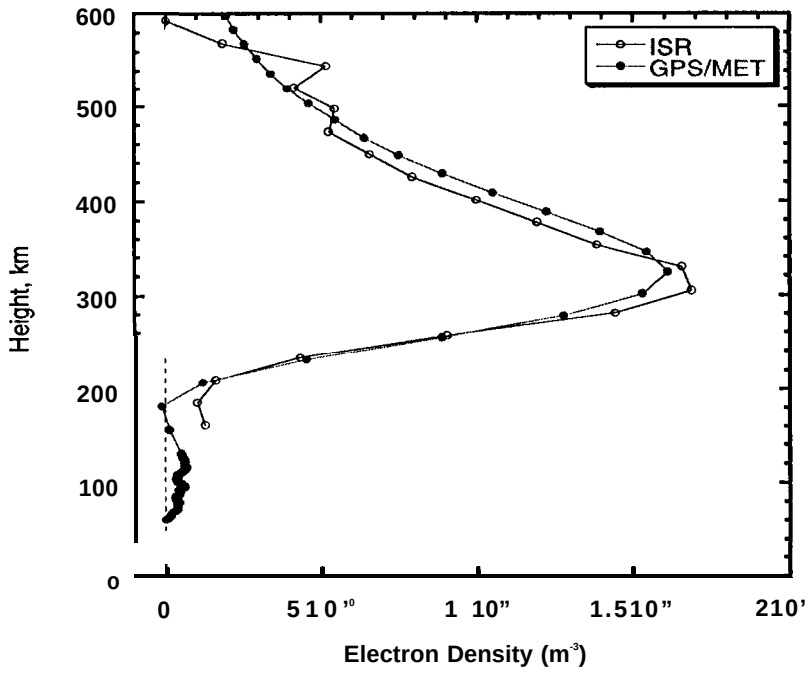
ISR
GPS/MET
Height, km
600
500
400
300
200
100
0
0
510'0
1 10"
1.510"
210'
Electron Density (m-3)

(b)

Figure 8

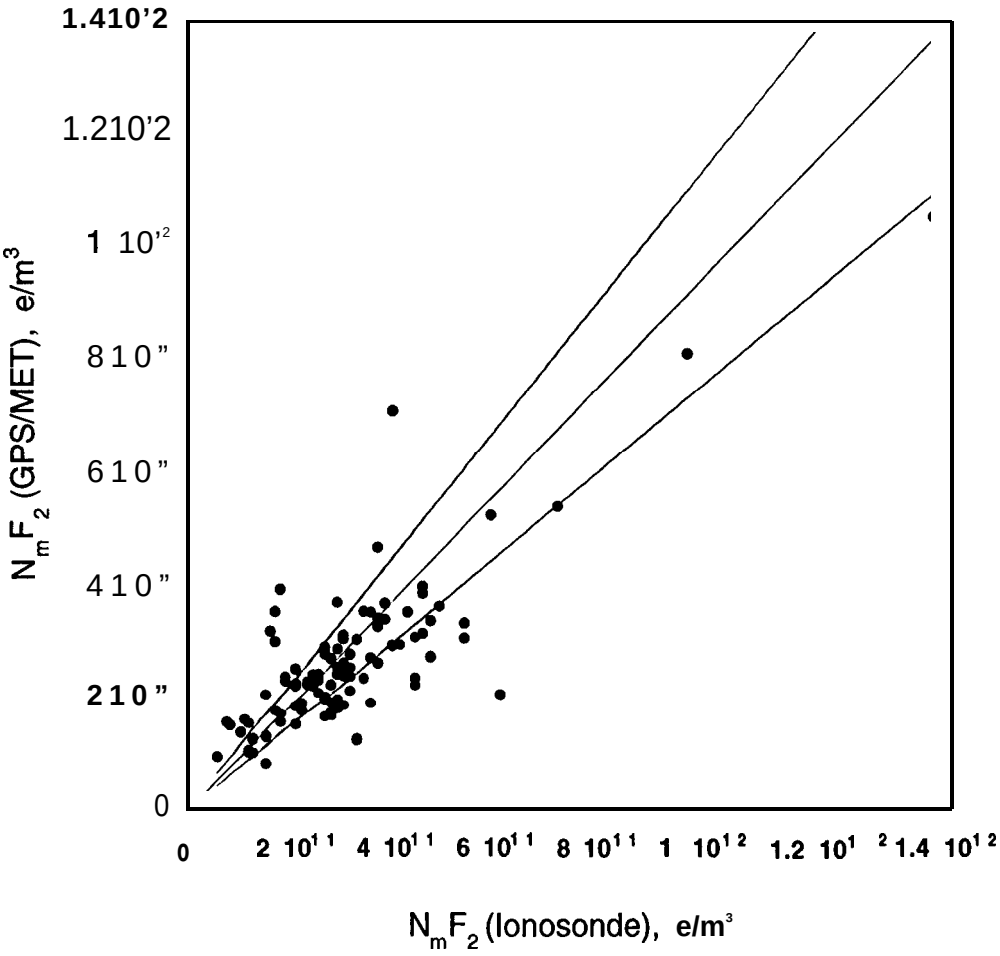
1.410'2
1.210'2
1 10'2
810"
610"
410"
210"
0
$N_m F_2$ (GPS/MET), e/m^3
0
2 10^{11}
4 10^{11}
6 10^{11}
8 10^{11}
1 10^{12}
1.2 10^{12}
1.4 10^{12}
$N_m F_2$ (Ionosonde), e/m^3

Fig. 9.a

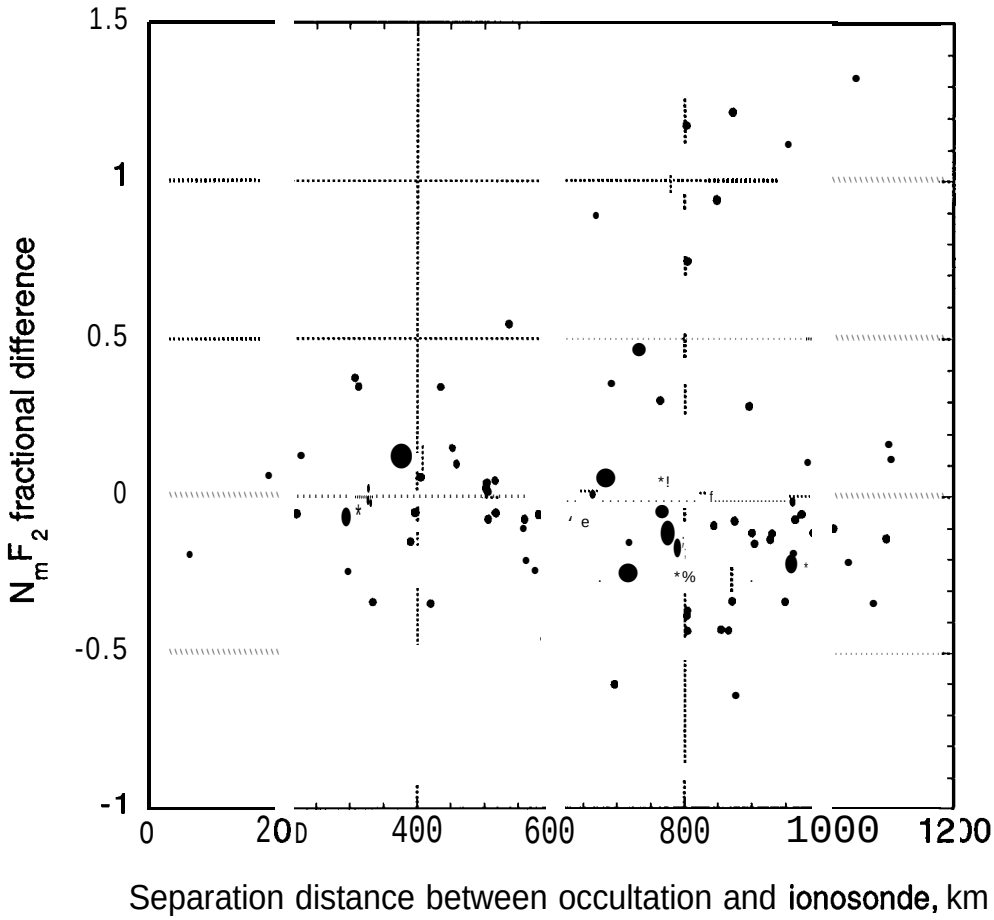
1.5
1
0.5
0
-0.5
-1
0
200
400
600
800
1000
1200
$N_m F_2$ fractional difference
Separation distance between occultation and ionosonde, km

Fig. 9.b

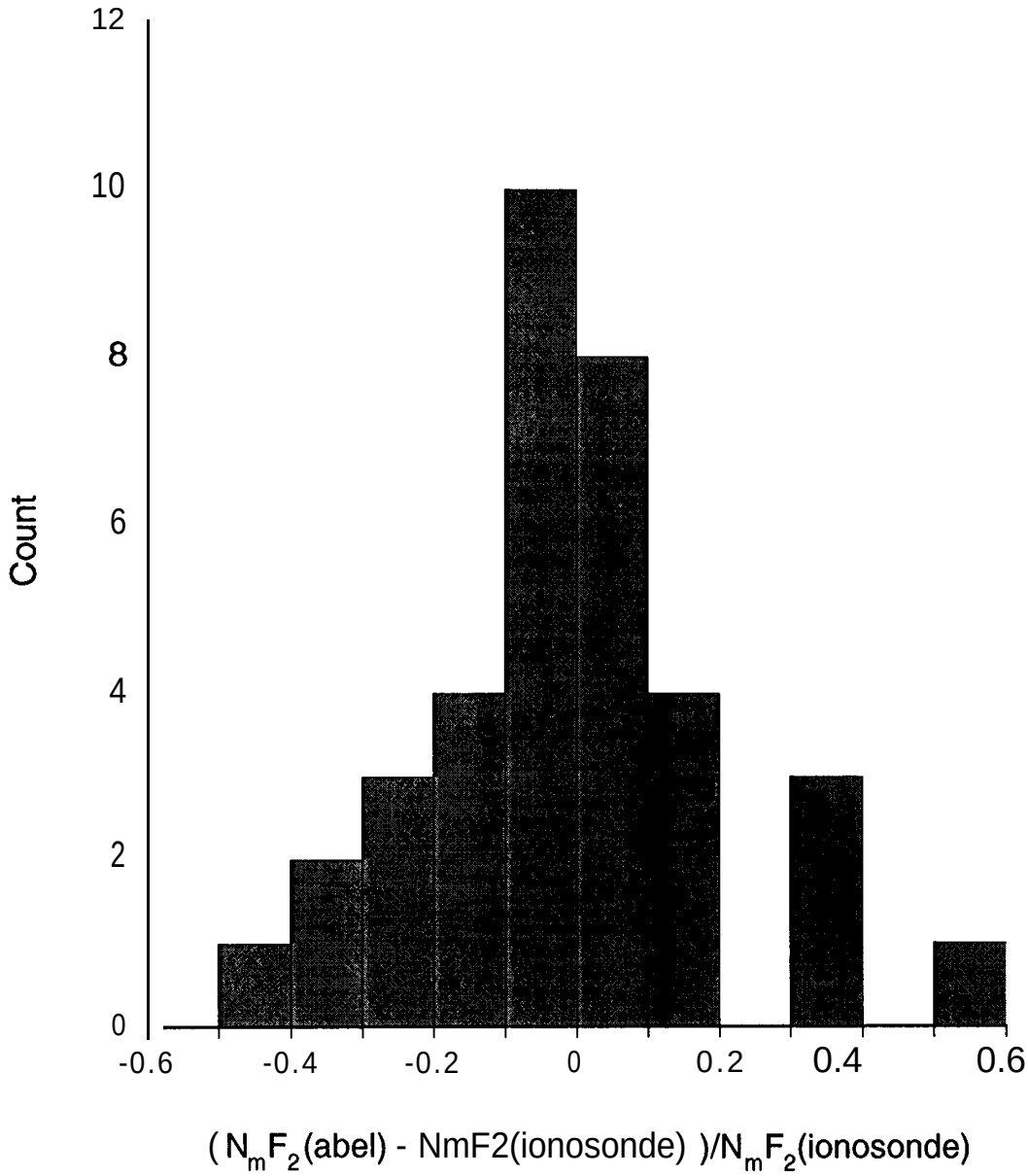
12
10
8
6
4
2
0
Count
-0.6
-0.4
-0.2
0
0.2
0.4
0.6
(NmF2(abel) - NmF2(ionosonde))/NmF2(ionosonde)

Fig. 10

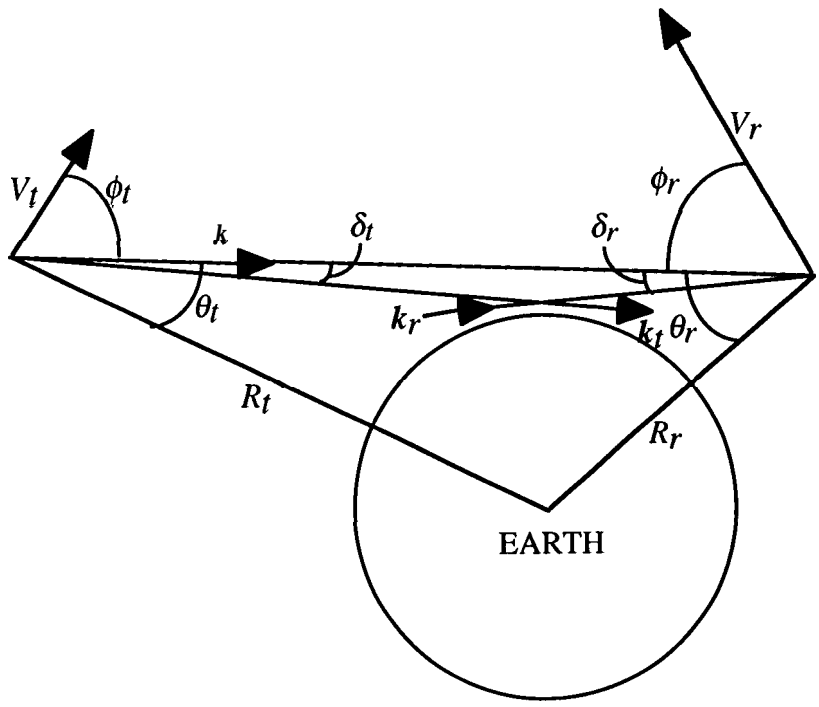
V_t
ϕ_t
k
δ_t
δ_r
V_r
ϕ_r
θ_t
k_r
k_t
θ_r
R_t
R_r
EARTH

Fig. A